ACS APPLIED ENERGY MATERIALS

www.acsaem.org Article

Compatibility of Various Electrolytes with Cation Disordered Rocksalt Cathodes in Lithium Ion Batteries

Jan-Paul Brinkmann, Niloofar Ehteshami-Flammer, Mingzeng Luo, Marco Leißing, Stephan Röser, Sascha Nowak, Yong Yang,* Martin Winter, and Jie Li*

Cite This: *ACS Appl. Energy Mater.* 2021, 4, 10909−10920 Read Online

ACCESS | Metrics & More | Article Recommendations | Supporting Information

ABSTRACT: Cation disordered rock salt cathode materials have gathered increased research interest over the last couple of years due to their high specific capacity and wide array of element combinations. It is still unclear whether the capacity fading observed for this type of material is solely due to the occurrence of anionic redox reactions and consequent material degradation or also due to the side reactions between the cathode material and the carbonate-based electrolyte. In order to address it, this study compares the differences in electrochemical performance of a rock salt $Li_{1.25}Fe_{0.5}Nb_{0.25}O_2$ cathode and cathode electrolyte interphase (CEI) formation in both lithium metal and lithium ion cells by using a conventional carbonate-based electrolyte and an ionic liquid-based electrolyte. Thereby, the ionic liquid electrolyte promotes capacity retention, whereas the organic carbonate-based electrolyte leads to increased capacity fading and ineffective CEI formation. Severe side reactions between the carbonate-based electrolyte and the cathode material are characterized by poor Coulombic efficiency and result in continuous inner resistance growth, ongoing gas evolution, and the coverage of the cathode surface with electrolyte degradation products like LiF and Li_2CO_3. This study shows the mismatch of carbonate-based electrolytes with the $Li_{1.25}Fe_{0.5}Nb_{0.25}O_2$ cathode and offers a strategy that can be also applied for the improvement of performance of other disordered rock salt cathode materials.

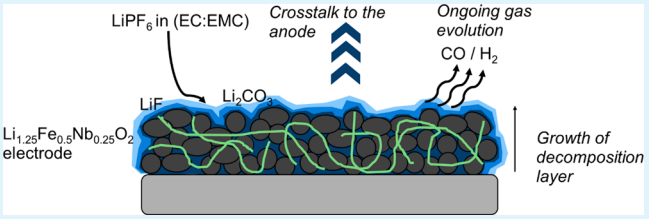

KEYWORDS: *disordered rock salt cathode, electrolyte decomposition, ionic liquid electrolyte, cathode electrolyte interface (CEI), anionic redox, lithium ion batteries*

1. INTRODUCTION

The demand for rechargeable batteries charged by renewable energy sources is steadily rising with the target of reducing carbon emission in cities, particularly during the operation of vehicles. Lithium ion batteries (LIBs) are still the most suitable technology for this task because of their overall better performance than other battery technologies.[1] Among all the components, cathode materials, because of their relatively low specific capacities (vs anode materials), represent the bottleneck for higher energy densities in LIBs.[2] Therefore, the development of cathode materials is the key strategy for further enhancement of energy density of LIBs.[3] State-of-the-art cathode materials for electric vehicles are mainly layered lithium transition metal (TM) oxides.[4] In order to achieve sufficient lithium transport properties, a stable layered structure has to be ensured during charge and discharge, which for the most part restricts the choice of the active TMs to combinations of Ni, Co, and/or Mn.[5] Other elements can be added to improve the overall material performance, but only in small quantities (commonly in the range of 1−5% by weight).[6,7] The limited element choice could ramp up the cost of the cathode material and eventually lead to shortages, especially for the less abundant Ni and Co in the near future.[8,9] A new class of cation disordered rock salt (DRX) cathodes have attracted research interest over the past few years and are less limited with regard to the active redox element.[10−12] Contrary to previous assumptions, these materials display reasonable lithium transportation properties, despite the lack of an ordered layered structure.[13] The Li-ion transport through DRX materials is facilitated by a percolating network of 0-TM transport channels present in these materials above a specific lithium threshold.[14,15] This discovery led to the study of a vast amount of possible synergies between different TMs, which then inspired the development of new chemistries for cathode application.[16−18] In recent years, the combination of a redox active TM with Nb as an inactive d^0 stabilizer has been discussed and evaluated.[19,20] Different TM choices thereby result in distinct and complex charge compensation mechanisms involving either sole cationic redox reactions or the combination of them and various degrees of anionic contribution to the material capacity. Research focus so far has been on the understanding of these intricate redox processes and the factors

Received: June 29, 2021
Accepted: September 7, 2021
Published: October 4, 2021

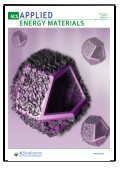

influencing them.[21] Little attention has been paid to the interactions between DRX materials and other components of a battery cell, for example, the electrolyte, the anode, and so on. It is still unclear if the relatively high potentials of the anionic redox displayed by these materials and the consequent high cut-off potentials during cell cycling are compatible with commercially used carbonate-based electrolytes and graphite anodes, or if unfavorable interactions among them exist and thus lead to the poor performance of some DRX materials.[22] In this study, a DRX material with a stoichiometry of $Li_{1.25}Fe_{0.5}Nb_{0.25}O_2$, which was previously reported to suffer from strong capacity fading and involve substantial amounts of anionic redox activity,[21] was used to investigate the compatibility of the DRX material with a conventional organic carbonate-based electrolyte. For comparison, this material was also studied in an ionic liquid (IL)-based electrolyte, which was used because of its presumed superior stability against oxidation and high potentials.[23−25] The surface of the cycled electrodes in these two electrolytes was thoroughly characterized, and thus, information regarding the mechanism of cathode electrolyte interphase (CEI)[26] formation and electrode degradation in conventional carbonate-based electrolytes is obtained. In addition, this study shows for the first time, to the best of our knowledge, the long-term performance of an LIB full cell configuration combining a DRX cathode with a graphite anode.

2. EXPERIMENTAL SECTION

2.1. Electrochemical Characterization. The $Li_{1.25}Nb_{0.25}Fe_{0.5}O_2$ active material was synthesized under the procedure that has been reported previously.[21] The electrode paste was prepared by mixing active material, carbon black (C-nergy Super C65, Imerys Graphite & Carbon), and polyvinylidene difluoride binder, (PVdF, Solef 5130, Solvay) in the weight ratio of 80:10:10 in *N*-methylpyrrolidone (NMP, anhydrous, 99.5%, Sigma-Aldrich) as solvent. In detail, the active material and the carbon black were pre-mixed in a swing mill (MM 400, Retsch) for 15 min at 15 Hz, then 30 min at 20 Hz, and 1 h at 30 Hz after adding PVdF and NMP. The obtained electrode paste was coated onto Al foil (20 μm, Evonik Industries) with a doctor blade in a wet thickness of 100 μm. After drying, the electrode sheet was punched into discs (Ø 12 mm) and pressed for 15 s at a pressure of 5 t. The mass loading of active material on each electrode is ≈2.3 mg/cm^2. For the preparation of graphite anodes, an electrode paste, which consists of graphite (SMGA4, Hitachi Chemical) Na-CMC (Walocel CRT 2000, Dow Wolff Cellulosics) and conductive carbon (C-nergy Super C65, Imerys Graphite & Carbon) in the weight ratio of 90:5:5 with distilled water as solvent, was coated onto copper foil (20 μm, Schlenck) with a wet thickness of 50 μm. The mass loading of active material on each electrode is ≈1.9 mg/cm^2.

The $Li_{1.25}Nb_{0.25}Fe_{0.5}O_2$ electrodes were built into Swagelock-type three-electrode[27] cells in a dry room (dew point <−60 °C) with Li metal disks (500 μm thick, battery grade, Albemarle Corporation) as negative (Ø 12 mm) and reference electrodes (Ø 8 mm) or CR2032-type two-electrode[27] coin cells (Tob New Energy) with graphite (Ø 12 mm) as the negative electrode. One layer of Whatman GF/D was used as separator in the Swagelock cells, whereas one layer of Freudenberg 2226 was used in coin cells. The conventional carbonate electrolyte used in this work is 1 M $LiPF_6$ in ethylene carbonate (EC): ethyl methyl carbonate (EMC) (3:7 wt %, battery grade, BASF SE), and the ionic liquid electrolyte is 0.5 M LiTFSI in *N*-propyl-*N*-methylpyrrolidinium bis(trifluoromethylsulfonyl)imide ($Pyr_{1,3}$TFSI). A total of 150 μL of the electrolyte was used for the Whatman GF/D separator and 50 μL for the Freudenberg separator. For *in situ* cell volume measurement and post-mortem investigation with scanning electron microscopy (SEM) and electrochemical impedance spectroscopy (EIS), pouch cells with a graphite (3 cm × 3 cm) negative electrode, $Li_{1.25}Nb_{0.25}Fe_{0.5}O_2$ (3 cm × 3 cm) positive electrode, Freudenberg 2226 (3.3 cm × 3.3 cm) separator, and 300 μL electrolyte were built. During cycling, the cells were fixed between two stainless steel plates.

2.2. X-Ray Powder Diffraction. X-ray powder diffraction (XRD) was conducted with a Bruker D8 Advanced (Ni-filtered Cu Kα radiation, λ = 0.154 nm) between 10° and 90° 2θ with a step size of 0.03° and a step time of 3 s.

2.3. X-Ray Photoelectron Spectroscopy. For the post-mortem X-ray photoelectron spectroscopy (XPS) measurements on the electrodes at different charge states, the cycled Swagelok cells were disassembled in a glovebox filled with argon (<1 ppm H_2O and O_2). The obtained electrodes were transferred into the XPS device, while avoiding any air contact using an argon filled antechamber and then left in the XPS chamber under turbomolecular vacuum for 12 h. The XPS characterization was conducted at a 0° angle of emission to the surface normal with a pass energy of 20 eV using a monochromatic Al Kα source ($h\nu$ = 1486.6 eV) at a 10 mA emission current and a 12 kV acceleration voltage (Axis Ultra DLD, Kratos). Additionally, a charge neutralizer was used for compensating the charging of the samples. To ensure the reproducibility, two or three spots were measured on each sample. Sputter depth profiling (SDP) was conducted *via* a monoatomic argon ion gun with argon gas as the ion source to probe deeper into the CEI bulk. The filament voltage was 0.5 kV with a sputter crater diameter of 1.1 mm, whereas the angle between the surface and the ion gun beam was 45°. The sputtering was conducted for 60, 180, and 780 s before XPS measurements, which were done with a 110 μm aperture and pass energy of 40 eV. The obtained spectra were analyzed with CasaXPS software. Electrodes that were in contact with the ionic liquid were washed 3 times with 200 μL of dimethyl carbonate (DMC) before the measurement.

2.4. Electrochemical Impedance Spectroscopy. EIS was performed using a BioLogic VMP III potentiostat in the frequency range of 0.1 MHz and 0.1 Hz and an amplitude of 10 mV. The measurement was first conducted at open circuit voltage before cycling and then repeated after every one of the 25 cycles. A 5 min rest was applied at the end of each charge/discharge to minimize the effect of polarization on the measurement.

2.5. Scanning Electron Microscopy. SEM images were taken with a Carl Zeiss Auriga Modular Crossbeam workstation, equipped with a Schottky field emission gun and a Gemini column as the electron source (3 kV, ≈ 3 mm working distance). The electrodes that were cycled in pouch cells containing either the carbonate-based or IL-based electrolytes were collected after 5, 25, 50, and 100 cycles and investigated with SEM. Electrodes that were in contact with the ionic liquid were washed 3 times with 200 μL of DMC beforehand to remove the nonelectron conductive liquid that would otherwise disturb the measurement by undesirable charging.

2.6. *In Situ* Cell Volume Measurements. Dahn et al.[28] have successfully tracked *in situ* gas volume change in a cell after various cycles using the Archimedean principle. Thereby, inspired by that work, the buoyant force of the cell suspended in water [MilliQ water, Merck Millipore Milli-Q Advantage A10, resistivity at 25 °C = 18.2 MΩ cm, total organic carbon ≤ 5 ppb] was measured with a Archimedes' *in situ* gas analyzer[29] using a small-scale thin film load cell (KD45 2 N, ME-Meßsysteme). Volume changes of the pouch cell influence the mass of the water that is replaced and therefore also the load detected by strain gauges in the measuring device. Through the calibration with a defined mass, the deformation of the strain gauges can be detected as voltage changes by a USB data acquisition module (OMB-DAQ-2408 Series, OMEGA Engineering GmbH), thus giving an exact value of the amount of gas that has evolved in the cell.

Gas chromatography barrier discharge ionization (GC-BID) detector GC measurements were done using a GC-2010 Plus system. A BID-2010 Plus (Shimadzu Deutschland was used as the detection unit) was used. The GC system was equipped with a PLOT gas separation column RT-Msieve 5A (30 m × 0.32 mm × 30 μm, Restek). To control the system, the LabSolutions software (version 5.90, Shimadzu) was used. The resulting chromatograms were evaluated with the Postrun Analysis editor (version 5.90, Shimadzu). A 25 μL gastight syringe was used to inject 5 μL into the GC system manually.[30]

https://doi.org/10.1021/acsaem.1c01879
ACS Appl. Energy Mater. 2021, 4, 10909−10920

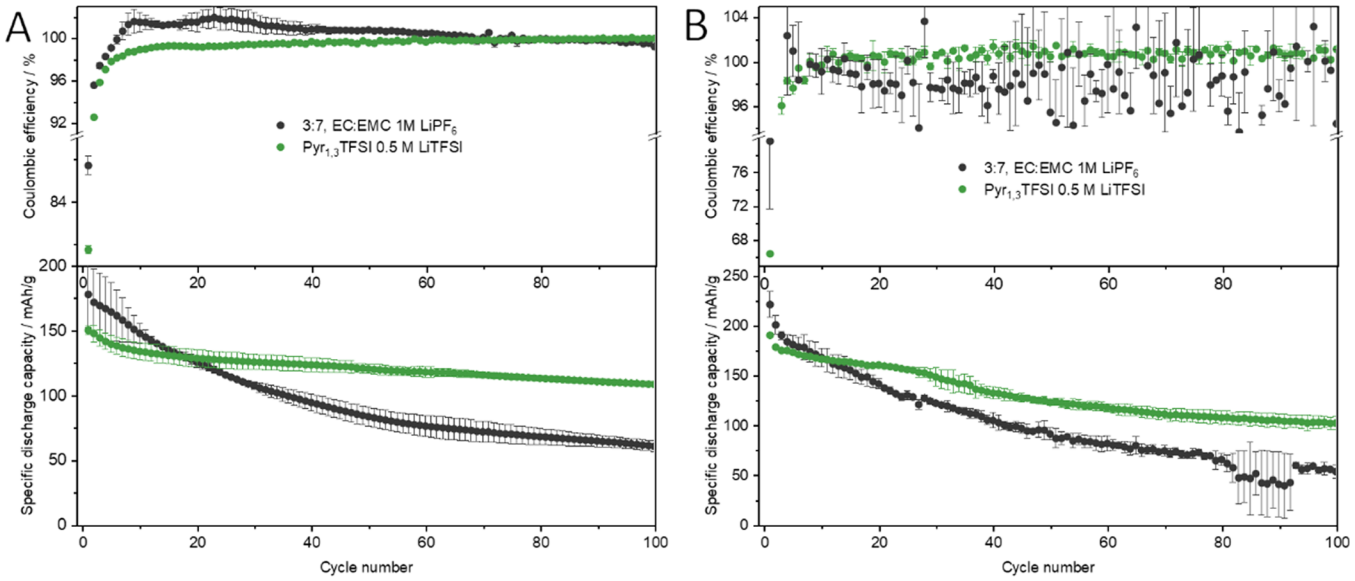

Figure 1. Electrochemical performance of $Li_{1.25}Nb_{0.25}Fe_{0.5}O_2$ || Li cells containing either a carbonate-based electrolyte or an ionic liquid-based electrolyte with a current rate of 1C at (A) 20 °C and (B) 40 °C.

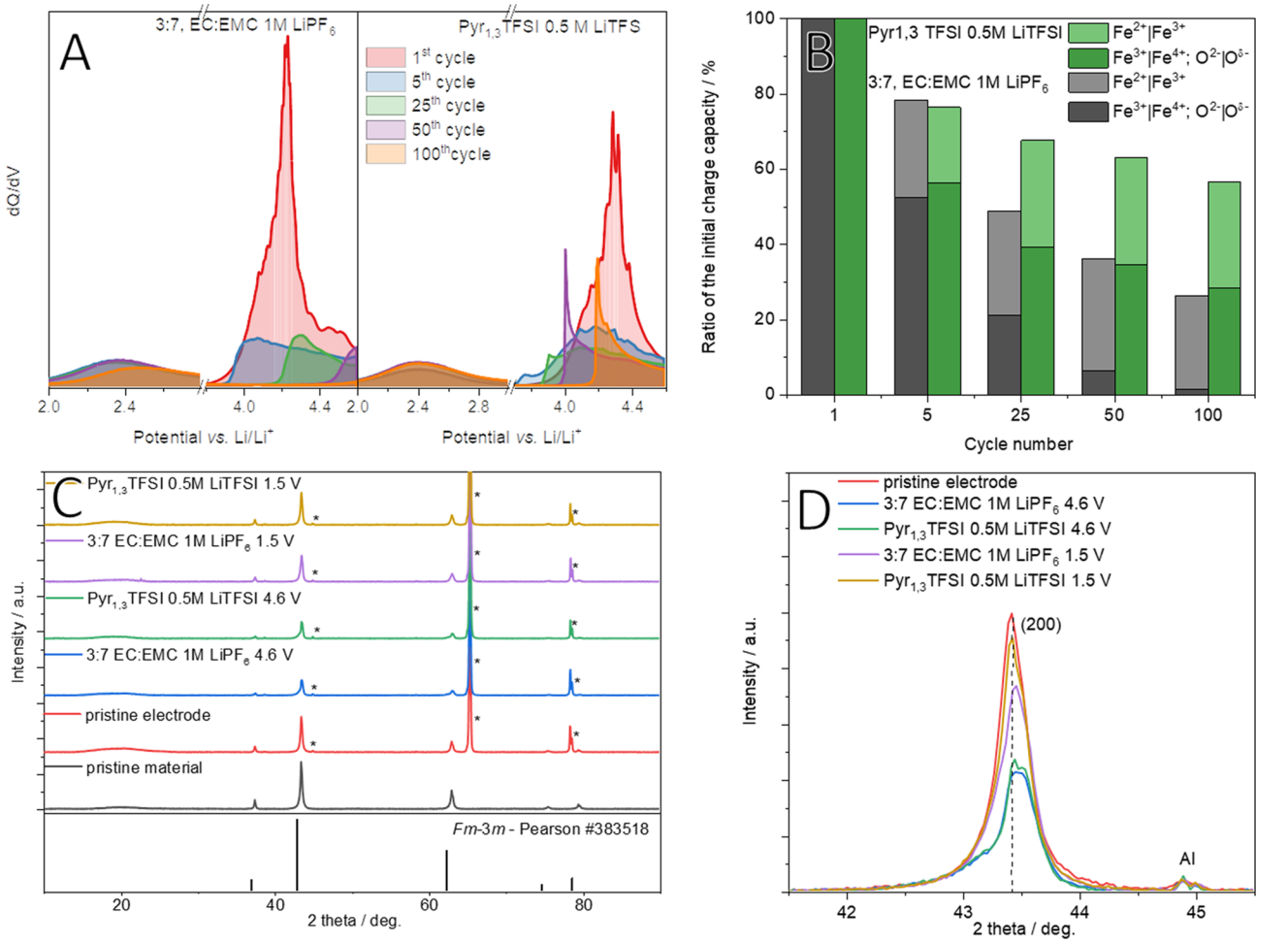

Figure 2. (A) Evolutions of oxidation peaks in the dQ/dV vs potential plots of $Li_{1.25}Nb_{0.25}Fe_{0.5}O_2$ with different electrolytes at different cycle numbers at 20 °C. (B) Contributions of cationic and anionic redox processes to the capacity, normalized to the initial values, at different cycle numbers. (C) XRD pattern of pristine $Li_{1.25}Nb_{0.25}Fe_{0.5}O_2$ and electrodes at different points of charge during the first cycle with either a carbonate-based or an IL-based electrolyte. Reflections caused by the Al current collector are marked with an asterisk. (D) (200) reflection of $Li_{1.25}Nb_{0.25}Fe_{0.5}O_2$ electrodes at different charge states during the first cycle with either a carbonate-based or an IL-based electrolyte.

https://doi.org/10.1021/acsaem.1c01879
ACS Appl. Energy Mater. 2021, 4, 10909−10920

3. RESULTS AND DISCUSSION

3.1. Electrochemical Performance of Lithium Metal Cells. As elaborated above, DRX cathodes suffer from substantial capacity fading often ascribed to be contributed by the surface reconstruction and/or oxygen loss from the material.[18] In addition to the inevitable reactions with the lithium metal anode,[31] an additional reason may be the occurrence of unfavorable side reactions of the cathode material with components of the carbonate-based electrolyte. In order to investigate this possibility, cells containing Li metal as the anode and $Li_{1.25}Nb_{0.25}Fe_{0.5}O_2$ cathodes were charged and discharged 100 times at 20 °C (Figure 1A) and 40 °C (Figure 2B) with a current of 0.1C (1C ≙ 300 mAh/g), respectively. The electrochemical performance of the cells containing the carbonate-based electrolyte (3:7, EC:EMC 1 M $LiPF_6$) is compared to those with an IL-based electrolyte ($Pyr_{1,3}TFSI$, 0.5 M LiTFSI). The presence of Fe in the material has a negative influence on the material performance because of its reductive coupling mechanism with lattice oxygen that can promote oxygen evolution, thus amplifying the side reactions of the material with the electrolyte.[32] As expected, the discharge capacity of the DRX material shows a rapid fading with the carbonate-based electrolyte even at 20 °C, losing 66% (117.5 mAh/g) of its initial discharge capacity over the course of 100 cycles. In contrast to that, cells with the IL-based electrolyte only lose 28% (41.73 mAh/g) of their initial discharge capacity and retain over 100 mAh/g at the end of 100 cycles. In the first 20 cycles, the cells containing IL electrolytes show lower discharge capacities due to the slow lithium transport kinetic caused by the higher viscosity of the ionic liquid.[33]

A look at Coulombic efficiencies (CEs) gives a first hint to the possible parasitic reactions with the electrolyte,[34] showing values above 100% for the carbonate-based electrolyte up to the 60th cycle. This can be caused by decomposition of the electrolyte during discharge, which generates a current that is not attributed to the lithiation of the cathode material. Such reactions are known to occur in Li||O_2 batteries, where the organic electrolyte is oxidized by oxygenated species during discharge.[35] The cells with ionic liquid-based electrolytes showing a CE of ≈99.6% (5th−100th cycle) do not show this behavior.

At 40 °C, all cells deliver higher initial discharge capacities, that is, 220 ± 12.9 mAh/g for those with the carbonate-based electrolyte and 190 ± 1.7 mAh/g for those with the IL-based electrolyte, mostly due to the faster lithium transport properties in the bulk of the cathode at higher temperatures.[36] The capacity difference for a specific cycle between the two electrolytes shrinks due to the faster decrease of viscosity and faster increase of ionic conductivity of the IL electrolyte at elevated temperatures. Additionally, capacity fading is heightened in both cases at elevated temperature; cells containing the carbonate-based electrolyte lose 76% (loss of 168.0 mAh/g, in average) of the initial discharge capacity, while those with the IL-based electrolyte lose 47% of the initial discharge capacity (88.2 mAh/g, in average) after 100 cycles. The CEs for both electrolytes at 40 °C show an unsteady behavior by reaching over 100% in several cycles, suggesting that the IL is also taking part in unfavorable side reactions at this temperature. Nevertheless, this behavior is more prominent for the carbonate-based electrolyte; thus, in order to pinpoint the electrolyte solvent that causes this behavior, EC and/or EMC were replaced by their fluorinated analogues FEC and FEMC.[37] The cycling performance of cells with various combinations of fluorinated carbonate solvent is shown in Figure S1. A more pronounced difference in cycling behavior can be observed at 40 °C. In addition, the more rapid fading and further deteriorated CE are detected from the cells containing FEC, while the replacement of EMC by FEMC has a much less impact on the electrochemical performance of the cells, suggesting that the cyclic carbonates are probably the course for the unfavorable side reactions.

Further understanding of the mechanism behind the capacity fade can be derived from the analysis of dQ/dV vs potential plots. Figure 2A shows the dQ/dV vs potential profiles of $Li_{1.25}Nb_{0.25}Fe_{0.5}O_2$ electrodes during the charge process depicted for selected cycles at 20 °C.

Thereby, the peak at ≈ 2.4 V can be attributed only to the cationic redox process in which Fe^{2+} is oxidized to Fe^{3+}. The redox mechanism behind the peak at a potential of 4.2 V vs Li|Li^+ is more complex and involves the oxidation of Fe^{3+} to Fe^{4+}, oxidation of O^{2-} to $O^{\delta-}$ and O_2, and the subsequent reduction of Fe^{4+} back to Fe^{3+} via a reductive coupling mechanism.[21] The Fe^{2+}|Fe^{3+} redox peak stays constant in intensity and potential for both electrolytes, with the only exception being that it shifts to slightly lower intensity and a higher potential at the 100th cycle in the carbonate-based electrolyte. In accordance with this, the capacity derived by integration of this peak is maintained at ≈25% of the initial charge capacity for both electrolytes, which is shown in Figure 2B. A more significant effect from the electrolyte is observed for the peak at ≈ 4.2 V vs Li|Li^+. For the carbonate-based electrolyte, this peak shifts to higher potentials along cycling and decreases in intensity till it is not noticeable anymore after 100 cycles. The significant decline in intensity leads to a decreased capacity from the redox reaction at this potential during cycling, which is also shown in Figure 2B. For the IL electrolyte, the loss of intensity and the shift to higher potential of this peak are both significantly diminished, and the capacity derived from it is still ≈28% of the initial charge capacity after 100 cycles. Overall, it can be established that the Fe^{2+}|Fe^{3+} redox couple at low potential is not affected during cycling and the capacity fading stems mostly from the redox process occurred at high potential (≈4.2 V vs Li|Li^+), which involves the electrochemical activities of lattice oxygen in combination with Fe^{3+}|Fe^{4+}. Comparing the two electrolytes, the cell with the IL electrolyte seems to be significantly less affected by this trend.

All reflections of the material displayed in Figure 2C can be assigned to the DRX structure *Fm*-3*m*. During charging and discharging, the intensity as well as the position of the reflection change with both electrolytes, as shown in Figure 4D for the (200) peak. Therefore, the shift to higher angles is observed before, which is presumed to be caused by the smaller ionic radii of oxidized Fe^{3+} and $O^{\delta-}$ species that emerge during charging, while the intensity decline is attributed to oxygen loss from the material.[21] During discharging, in contrast to the carbonate-based electrolyte, the intensity and position of reflections from the material cycled in the IL-based electrolyte shift more to their initial pristine state, which is a further evidence for a more reversible redox reaction.

3.2. CEI Evolution on the DRX Cathode. In order to identify the reaction products forming in the CEI at the cathode| electrolyte interface during cycling, XPS measurements with SDP were conducted on $Li_{1.25}Nb_{0.25}Fe_{0.5}O_2$ electrodes cycled in both electrolytes at the charged and discharged states. Signals from Nb and lattice oxygen in their respective Nb 3d and O 1s spectra can be detected on a pristine electrode surface without

https://doi.org/10.1021/acsaem.1c01879
ACS Appl. Energy Mater. 2021, 4, 10909−10920

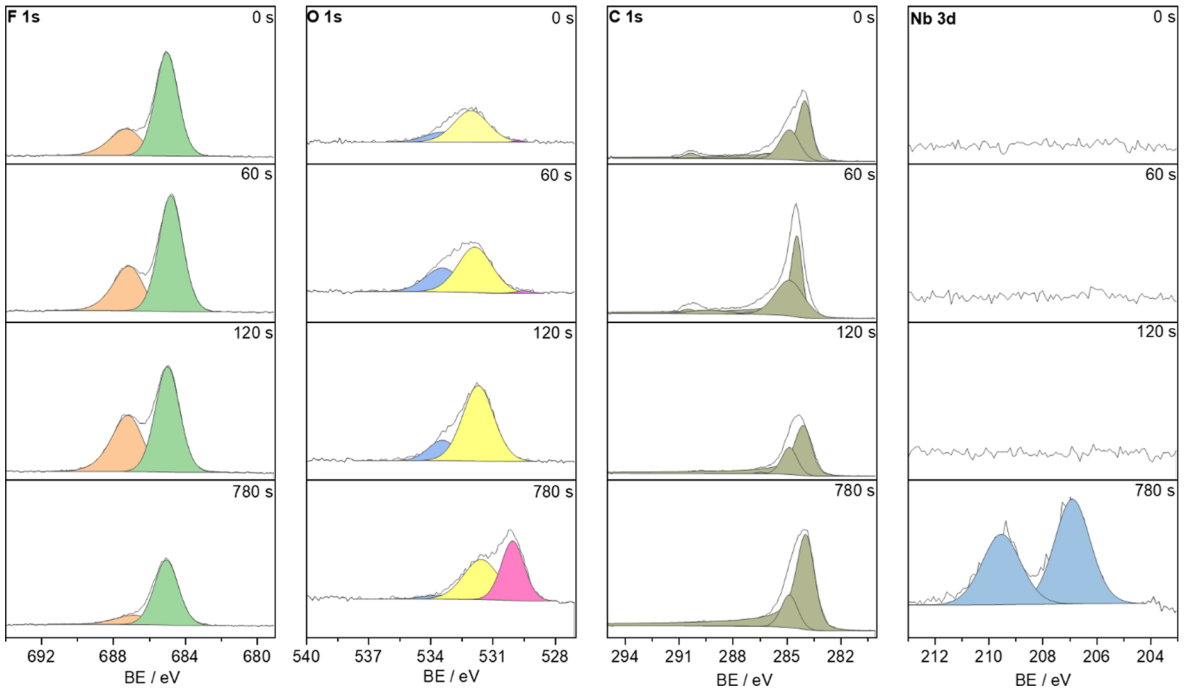

Figure 3. F 1s, O 1s, C 1s, and Nb 3d XPS spectra of the $Li_{1.25}Nb_{0.25}Fe_{0.5}O_2$ cathode after storage for 100 h at 20 °C in a cell with a carbonate-based electrolyte.

sputtering (see Figure S2). The spectra of the electrode stored in the carbonate-based electrolyte are displayed in Figure 3. In the F 1s spectra, the higher binding energy peak is attributed to PVdF and $LiPF_6$ and the lower one corresponds to LiF, resulting from $LiPF_6$ reduction.[38] In the O 1s spectra, the two signals at high binding energy, that is, 534.0 and 532.0 eV, are assigned to organic carbonates (R_2CO_3) and Li_2CO_3, respectively, with the latter one (for Li_2CO_3) being more pronounced. Meanwhile, the peak at the 529.5 eV, which is assigned to lattice oxygen in $Li_{1.25}Nb_{0.25}Fe_{0.5}O_2$ and Li_2O, does not show up until the 780 s sputtering is conducted. This finding proves that CEI can be directly formed on the DRX electrode surface by contacting with the carbonated-based electrolyte and also indicates Li_2CO_3 as one component of the CEI layer that can be oxidized at high voltages during charging, which would result in a decreased CEI thickness, in agreement with previous reports.[39−41] In the C 1s spectra, in order to eliminate the error caused by overlapping of the peaks corresponding to amorphous carbon, conductive carbon, and binders, they are not fitted individually and the sum of their contributions were used for interpretation, the details of which are given in Figure 4. In accordance with the peak for lattice oxygen in the O 1s spectra, characteristic peaks of Niobium could only be detected after 780 s of sputtering, again suggesting the formation of a CEI on the cathode surface.

To investigate the effect of charge/discharge processes on CEI composition, the depth-dependent evolution of the atomic concentration of F, O, C, and Nb in the surface layer of the electrode cycled either in a carbonate-based or in an IL-based electrolyte was determined from XPS spectra along with sputtering time. The studies were carried out on the electrodes at both ends of charge (4.6 V vs $Li|Li^+$) and discharge (1.5 V vs $Li|Li^+$) after four complete cycles, and the results are shown in Figure 4. The atomic concentrations of S and N in the case of the IL were negligible and are not shown here. Due to the surface sensitivity of the XPS technique, the atomic concentrations of the lattice oxygen and Nb can be used to evaluate the thickness of the CEI,[42] specifically for this material. In the case of the carbonate-based electrolyte, these signals only show up after 720 s of sputtering, which implies a sizable surface layer. Thereby, the thickness seems to increase during discharge, as indicated especially by the decreased concentration of Nb in this state. Besides the increased concentration of lattice oxygen and Nb after 780 s sputtering, the intense amount of LiF on the electrode surface is found to be significantly diminished at the charged state after 780 s of sputtering. Meanwhile, the concentration of LiF as well as Li_2CO_3 after discharge is lower compared to the charged state, which suggests that the CEI at this state consists of more organic compounds. Some of these organic compounds can detach from the surface through oxidation at high voltages, which uncovers a more LiF-rich CEI. Additionally, higher concentration of LiF at the charged state can be tied to reactions of the electrolyte solvents with oxygenated species creating LiF in a subsequent reaction step, which was observed for cathode materials with anionic redox behavior before.[43]

Figure S3 depicts the atomic concentration of LiF and Li_2CO_3 after 25 cycles. Interestingly, the concentration of LiF increases after the first sputtering steps and decreases again after 720 s, which indicates that the composition of the CEI formed in the carbonate-based electrolyte varies substantially with depth, Li_2CO_3 can be found more at the surface, and higher concentrations of LiF are present in deeper regions of the CEI, closer to particles of the cathode material. On the surface of the electrode cycled in the IL electrolyte, less contents of LiF and higher amounts of carbon species were detected. Contrary to the carbonate-based electrolyte, signals from lattice oxygen and Nb in the material could be detected on the surface of electrodes (0 s) in both charged and discharged states. This indicates a much thinner CEI layer formed when cycling in the IL electrolyte. In addition, the atomic concentration of the detected species of electrodes cycled with the IL electrolyte generally shows only insignificant differences compared to those with the

https://doi.org/10.1021/acsaem.1c01879
ACS Appl. Energy Mater. 2021, 4, 10909−10920

Figure 4. Evolution of depth-dependent atomic concentration of F, O, C, and Nb on the $Li_{1.25}Nb_{0.25}Fe_{0.5}O_2$ cathode surface layer after five cycles with the carbonate-based electrolyte in their charged (4.6 V vs Li|Li$^+$) and discharged (1,5 V vs Li|Li$^+$) states or the IL-based electrolyte in their charged (4.6 V vs Li|Li$^+$) and discharged (1.5 V vs Li|Li$^+$) states.

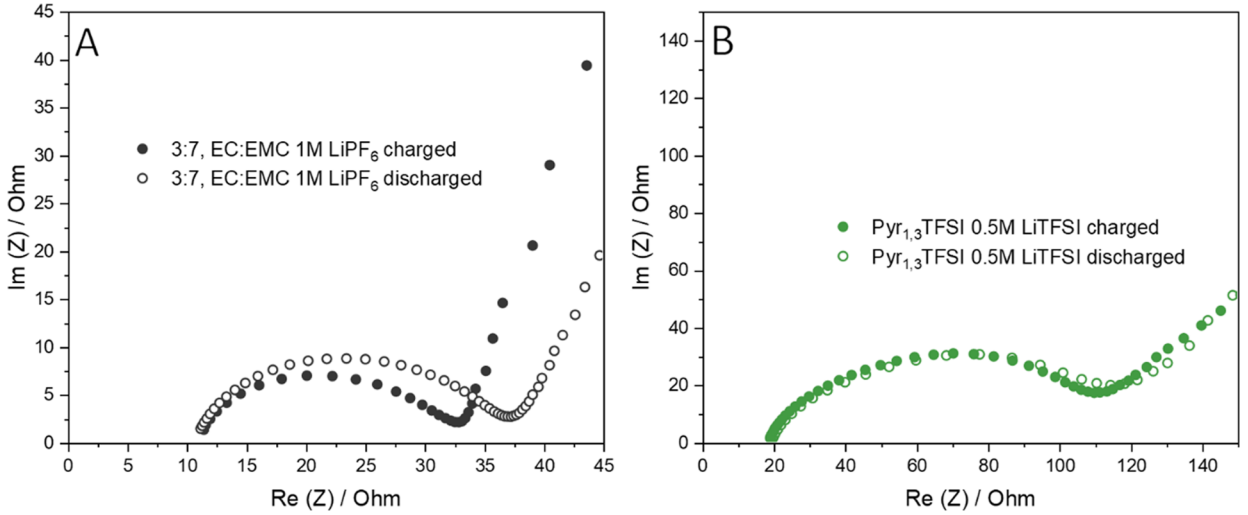

Figure 5. EIS Nyquist plots of $Li_{1.25}Nb_{0.25}Fe_{0.5}O_2$ || Li cells with (A) organic carbonate solvent-based electrolyte or (B) ionic liquid-based electrolyte during the fifth cycle. The solid circles represent the plots at 4.6 V in the charged state, and the hollow circles represent those at 1.5 V in the discharged state.

carbonate-based electrolyte, independent of the state of charge (SoC), suggesting only minor changes in the formed CEI during cycling. Overall, it can be concluded that the CEI on the $Li_{1.25}Nb_{0.25}Fe_{0.5}O_2$ cathode formed in the presence of ILs is

https://doi.org/10.1021/acsaem.1c01879
ACS Appl. Energy Mater. 2021, 4, 10909−10920

much thinner and also shows less evolution and growth with ongoing cycling than the carbonate-based electrolytes.

In situ EIS measurements were carried out in two-electrode $Li_{1.25}Nb_{0.25}Fe_{0.5}O_2$ || Li cells with either a carbonate-based electrolyte or an IL-based electrolyte. The measurement was conducted when the cell was charged to 4.6 V and discharged to 1.5 V, and the resulting Nyquist plots are shown in Figure 5. An obvious impedance difference between the charged and the discharged state can be observed from the cell in contact with the carbonate-based electrolyte (Figure 5A), which is consistent with the results of XPS, which showed that the CEI formed in this cell is not effective and evolves during cycling. Interestingly, the alternate behavior between higher and lower resistances in the discharged and charged cells is repeated for the whole measurement duration of 25 cycles (Figure S4). Therefore, the resistance of the cell increases during discharge and decreases during the following charge process. Due to fitting the results with a physical model (Figure S4D), it is possible to differentiate between the individual resistances of the electrolyte (R_e), the surface layer (R_f), and the charge transfer (R_{ct}). While in Figure 4B both R_e and R_{ct} remain constant compared to the charged and discharged state of the same cycle, the alternating behavior is shown by the surface layer resistance. Because in the same cycle, the CEI layer is thicker at the end of discharge than at the end of charge, as has been proven by XPS (Figure 4), this alternate resistance behavior leads to a speculation that part of the components of CEI may release from the electrode surface or dissolve in the electrolyte during the charging process. The cell with the IL electrolyte, on the other hand, shows a similar impedance in both SoCs (Figure 5B). All three resistances (Figure S4C) display a constant behavior in both charge states. The higher overall impedance of the cell with the IL electrolyte compared to the carbonate-based electrolyte can be ascribed to the interactions with the lithium metal anode rather than with the DRX cathode. This becomes clear when taking a look at symmetrical cathode || cathode cells (see Figure S5), which show smaller impedances with the ionic liquid-based electrolyte as with the carbonate-based electrolyte. Combining the XPS and EIS results, an illustration of CEI evolution on the DRX electrode when using carbonate-based electrolyte is depicted in Figure 6. It can be concluded that the carbonate-based electrolyte is not able to form an effective CEI on the DRX cathode material, but instead reacts constantly with its surface, forming and decomposing a surface layer that consists of LiF, Li_2CO_3, and other carbonaceous compounds. These reactions occur at high voltage not only during charging, but also during discharging. Some carbonaceous compounds though their formula cannot be identified in this work, release from the electrode surface resulting in a thinner and more LiF-rich CEI layer at the end of charging. The IL-based electrolyte, on the other hand, shows negligible reactions between the DRX electrode and electrolyte.

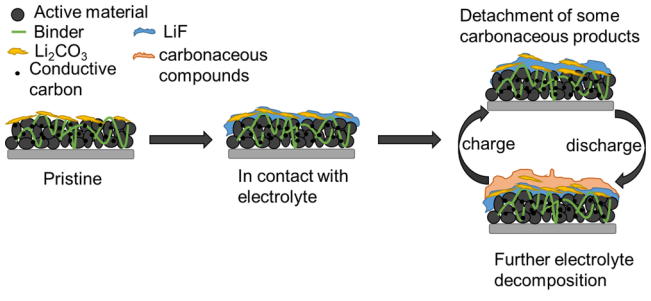

Figure 6. Reaction scheme of the carbonate-based electrolyte with the $Li_{1.25}Nb_{0.25}Fe_{0.5}O_2$ cathode material. CEI formation starts when the electrode is in contact with the electrolyte. During cycling, ongoing further electrolyte decomposition leads to a thicker CEI in the discharged state, while at high voltages of the charge state, some of the carbonaceous products release from the electrode surface and more LiF is exposed. This leads to a thinner LiF-rich CEI at high potentials.

3.3. Electrochemical Performance in Lithium Ion Full Cells. Figure 7 compares the electrochemical performance of $Li_{1.25}Nb_{0.25}Fe_{0.5}O_2$ || graphite cells using either carbonate-based or IL-based electrolytes. The cells were cycled for 100 cycles both at 20 °C (Figure 7A) and at 40 °C (Figure 7B). To our knowledge, it is the first report on the long-term performance of lithium ion full cells containing a DRX cathode material. Because of the incompatibility of the pure IL electrolyte with the graphite anode, 10 wt % of EC was added to the IL-based electrolyte to ensure an effective solid electrolyte interphase (SEI)[44] formation on the anode and prevent exfoliation of the graphite due to co-intercalation of the large pyrrolidinium ion.[45] Similar to the results obtained from lithium metal cells, the lithium ion cell with the IL electrolyte shows reduced capacity fading both at 20 and at 40 °C when compared with those with the carbonate-based electrolyte, even though the initial discharge capacities are lower because of the higher viscosity of the IL. The material can retain 48.9% (74.7 ± 2.92 mAh/g, 20 °C) and 31.7% (53.9 ± 6.07 mAh/g, 40 °C) of its initial discharge capacity when cycled with the IL-based electrolyte, but it decreases to 39.8% (65.8 ± 7.52 mAh/g, 20 °C) and 13.0% (24.0 ± 3.38 mAh/g, 40 °C) when cycled with the carbonate-based electrolyte. Significant differences can also be detected in the respective CEs of the cells. The average CE (5th to 100th cycle) at 20 °C for the carbonate-based electrolyte is 98.6 ± 0.3%, which increases to 99.2 ± 0.2% for the IL electrolyte. Elevated temperatures of 40 °C cause a further decrease in the average CE to 96.1 ± 0.4% for the carbonate-based and 98.1 ± 0.9% for the IL-based electrolyte. This leads to the conclusion that the decomposition of both electrolytes is elevated at higher temperature. Nevertheless, the IL-based electrolyte contributes to a more stable and efficient cycling of the DRX cathode material. The addition of EC enabling effective SEI formation on graphite is necessary for successful application in lithium ion cells.

3.4. CEI Evolution on the DRX Cathode in Lithium Ion Full Cells. Figure 8A,B depicts the respective Nyquist plots for cells with one of the two electrolytes for the first 25 cycles. The impedance was measured after the cells reached a cut-off voltage of 4.6 V during charging and 0.5 V during discharging. It can be seen in Figure 8C that the charge transfer (R_{ct}) and surface film resistance (R_f) of the cell with the carbonate-based electrolyte continuously increase, while those of the cell with the IL electrolyte, on the other hand, change only slightly at the beginning of cycling and then reach a plateau at around 10 Ω. This is further evidence for decreased side reactions between the DRX cathode and electrolyte when using the IL-based electrolyte instead of the carbonate-based electrolyte. Similar trends can be seen for the impedance in the charged state at 20 °C (Figure S6) and 40 °C (Figure S7), where the carbonate-based electrolyte also shows a steady increase in impedance. Therefore, the rising surface layer resistance, as shown in Figure S6C, is the main reason for the impedance growth in $Li_{1.25}Nb_{0.25}Fe_{0.5}O_2$ || Graphite cells with carbonate electrolytes.

In order to illustrate the surface evolution of the CEI during cycling, the DRX cathode electrodes were investigated with

https://doi.org/10.1021/acsaem.1c01879
ACS Appl. Energy Mater. 2021, 4, 10909−10920

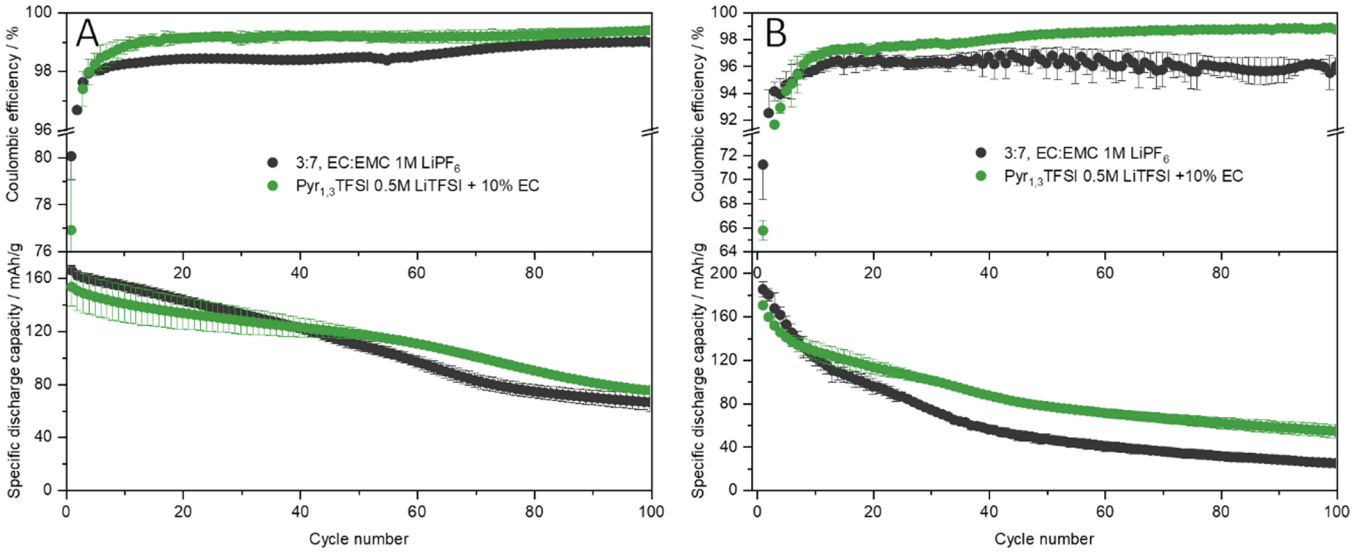

Figure 7. Coulombic efficiencies and specific discharge capacities of lithium ion cells containing a $Li_{1.25}Nb_{0.25}Fe_{0.5}O_2$ cathode, a graphite anode, and either a carbonate-based electrolyte or an ionic liquid-based electrolyte with a current rate of 0.1C at (A) 20 °C and (B) 40 °C.

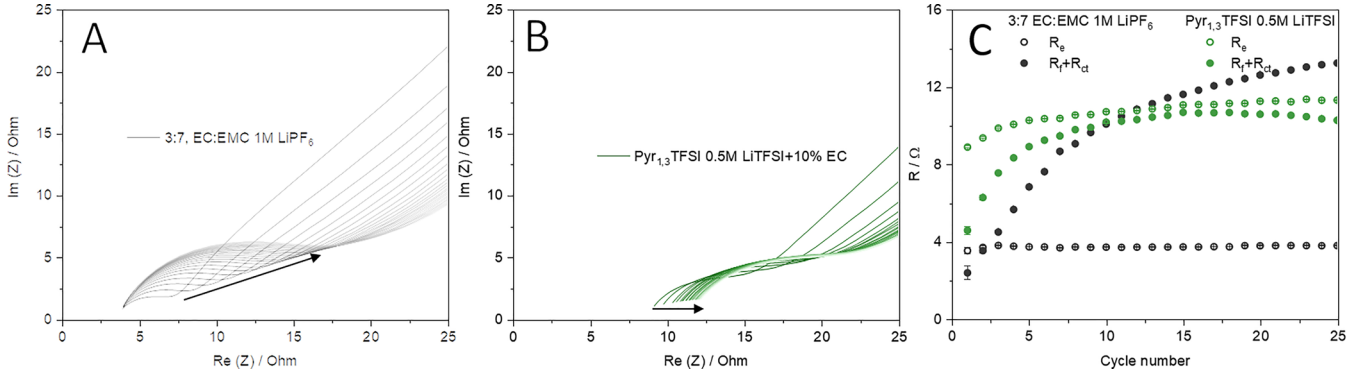

Figure 8. Evolutions of EIS Nyquist plots of $Li_{1.25}Nb_{0.25}Fe_{0.5}O_2$ || Graphite cells with (A) carbonate-based electrolyte or (B) an ionic liquid-based electrolyte over the course of 25 cycles. (C) Evolution of electrolyte resistance (R_e) and the combination of charge transfer and surface film resistance ($R_f + R_{ct}$) in $Li_{1.25}Nb_{0.25}Fe_{0.5}O_2$ || Graphite cells.

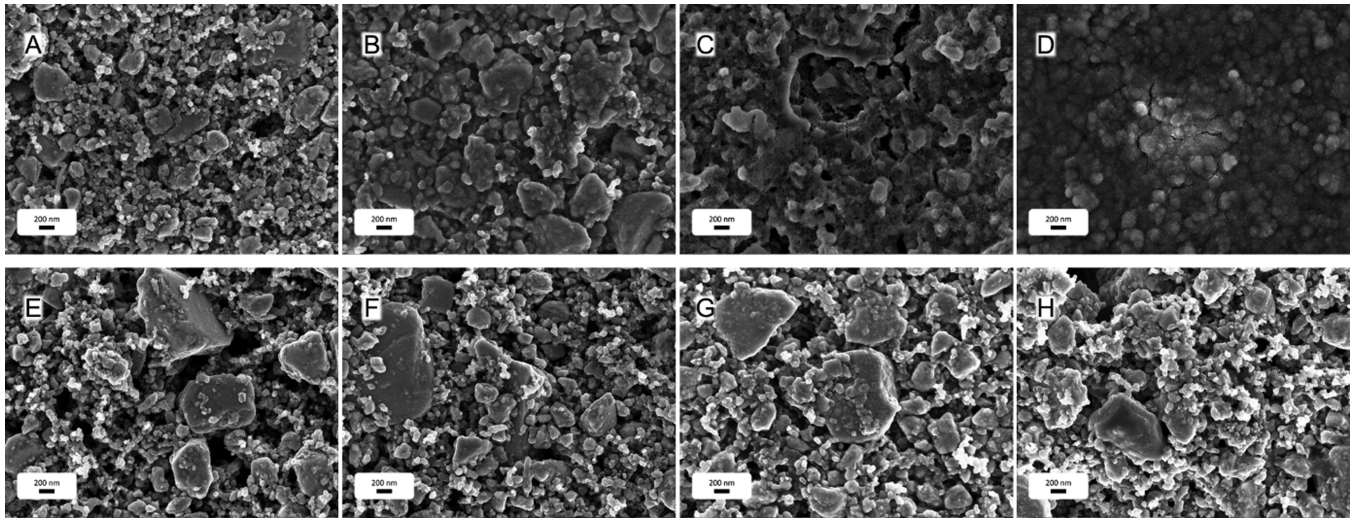

Figure 9. SEM images of the surface of a $Li_{1.25}Nb_{0.25}Fe_{0.5}O_2$ cathode after cycling in either a carbonate-based electrolyte (A–D) or an ionic liquid-based electrolyte (E–H). The images represent different cycle numbers such as 5 cycles (A,E), 25 cycles (B,F), 50 cycles (C,G), and 100 cycles (D,H).

SEM after 5, 25, 50, and 100 cycles in either the carbonate-based and IL-based electrolyte. The results are depicted in Figure 9. After five cycles, both electrodes (Figure 9A,E) show a clean surface independent of the choice of electrolyte. The

https://doi.org/10.1021/acsaem.1c01879
ACS Appl. Energy Mater. 2021, 4, 10909−10920

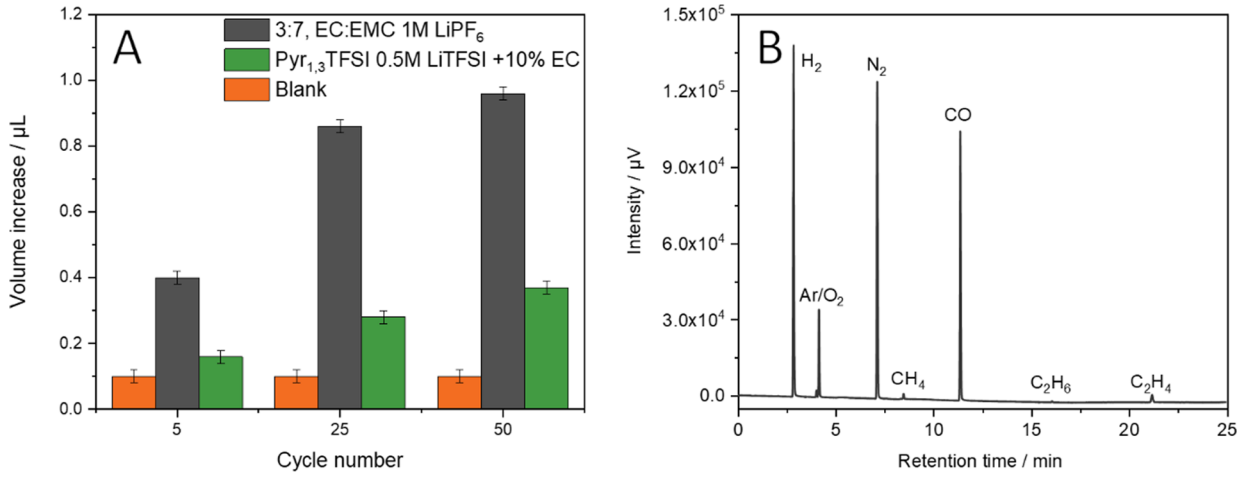

Figure 10. (A) Volume increase in lithium ion pouch cells cycled with a carbonate-based on an ionic liquid-based electrolyte after 5, 25, and 50 cycles measured by the Archimedean principle. For comparison, a blank cell without an electrolyte was stored for the same time and measured accordingly. (B) GC-BID chromatogram of the gases formed within the carbonate electrolyte containing pouch cells after 50 cycles.

degradation of the electrode surface is first seen after 25 cycles with the carbonate-based electrolyte (Figure 9B), on which some pores in the electrode are clogged by decomposition products. This trend is then continued at 50 cycles (Figure 9C), where most particles on the electrode surface are covered by deposition products. Then, a remarkable change is visible after 100 cycles (Figure 9D), where the whole electrode surface is covered with a thick layer and no pore can be observed anymore. This leads to the conclusion that decomposition of the carbonate-based electrolyte happens continuously during cycling; thus, the CEI layer on the DRX surface that is constructed by the occurrence of these side reactions is unstable and grows accordingly. For the IL electrolyte, on the other hand, degradation of the electrode surface is not visible and no pores are clogged even after 100 cycles.

A similar trend can be seen on the anode side (Figure S8), where the use of the carbonate-based electrolyte in the cells leads to thick surface deposition on top of the graphite particles. Because a comparable degree of degradation of the graphite anode was observed in carbonate-based electrolytes cycled with conventional cathode materials, when a crosstalk from the cathode to the anode is present,[46,47] such a transfer of decomposition products is also suggested here as a possible explanation. Because parasitic reaction with the electrolyte often causes the evolution of gases,[48] pouch bag cells containing the DRX cathode and graphite anode were assembled and cycled for 5, 25, and 50 cycles to track the gas volume change inside the cell using the Archimedean principle. For comparison, the volume change of a blank cell without the electrolyte was also measured after 100, 500, and 1000 h, which correspond to the completion of 5, 25, and 50 cycles at the rate of 0.1 C. The results are depicted in Figure 10 A. The blank cell increases its volume by 0.1 ± 0.02 μL after storing for 100 h (equal to 5 cycles) and does not change with prolonged storage time, indicating that the assembled pouch cells are tight and no atmosphere can penetrate into the cell. The volume of the pouch bag cell containing IL increases its volume slightly with 0.16 ± 0.02 μL, 0.28 ± 0.02 μL, and 0.37 ± 0.02 μL after 5, 25, and 50 cycles, respectively. A more notable increase can be detected for the cell with the carbonate-based electrolyte, which show a volume increase of 0.40 ± 0.02 μL after 5 cycles, which is already higher than the volume change of the cell containing IL after 50 cycles. The volume increase maintains a fast pace till 25 cycles (0.86 ± 0.02 μL) and slows down afterward (e.g., 0.96 ± 0.02 μL after 50 cycles). The volume change is clearly contributed by the gas evolution from the electrolyte decomposition, which brings a safety concern leading to a potential rupture of the cell. The composition of the gas phase from the cell cycled with the carbonate-based electrolyte for 50 cycles is then investigated by GC-BID. The resulting chromatogram is depicted in Figure 10B. The gas amount was not sufficient to measure in cells containing the IL electrolyte, which also indicates a stable cell system. The presence of N_2 and O_2 can be explained by contamination with the surrounding atmosphere during sample preparation before the measurement. H_2 and CO as well as CH_4, C_2H_6, and C_2H_4 stem from SEI and CEI formation as well as ongoing reactions inside the cell during cycling and are common products in gas phases of LIBs.[49] Thereby, CO can be obtained by oxidation of electrolyte decomposition products and EC during charging. This gas evolution in the charge process may result from the loss of surface compounds thus the thinner surface layer, that was being discussed in lithium metal cells. A more significant finding is the increased share of H_2 ($68.0 \pm 0.23\%$) in the overall gas phase. Recent studies suggest the reduction of electrolyte decomposition products that are generated by the oxidation of EC on the cathode side as the main source for H_2 evolution in LIBs.[50,51] This assumption is in agreement with the results presented in this study, suggesting that the side reactions between the DRX electrode and electrolyte components, especially EC, take the main responsibility for the decreased performance of the lithium ion cell with DRX cathodes.

4. CONCLUSIONS

The performance of the $Li_{1.25}Nb_{0.25}Fe_{0.5}O_2$ DRX cathode material and its interactions with the electrolyte are thoroughly investigated. In general, carbonate electrolytes on their own are not suitable for use with DRX materials. Their combination results in cells showing rapid capacity loss due to the poor reversibility of $Fe^{3+}|Fe^{4+}$ and anionic redox as well as the harsh side reactions between the DRX electrode and electrolyte. The products from these side reactions, including LiF, Li_2CO_3, and carbonaceous compounds, detach and re-form along cycling, lead to coverage of the surface with an ineffective CEI, and clog the pores of the DRX electrode. These findings are more severe

https://doi.org/10.1021/acsaem.1c01879
ACS Appl. Energy Mater. 2021, 4, 10909−10920

at elevated temperatures, for example, 40 °C, and can be mitigated by swapping the carbonate-based electrolyte with an IL-based electrolyte, even though more work must be done regarding the low ionic conductivity, high viscosity, and poor compatibility with the graphite anode of ILs. Meanwhile, the critical gas evolution from cells containing the carbonate electrolyte is significantly limited by this swap, which is also promising from the viewpoint of safety. Once IL-based electrolytes become cost-competitive, this work will increase the potential of practical application of the DRX material and will show a way to enhance the performance on their cell level besides changes of the cathode material.

■ ASSOCIATED CONTENT

Supporting Information

The Supporting Information is available free of charge at https://pubs.acs.org/doi/10.1021/acsaem.1c01879.

Cycling performance of the $Li_{1.25}Nb_{0.25}Fe_{0.5}O_2$ cathode in fluorinated electrolytes; XPS spectra of a pristine cathode; atomic concentration of fluorine- and oxygen-containing species after 25 cycles in a carbonate electrolyte; EIS results and model of $Li_{1.25}Nb_{0.25}Fe_{0.5}O_2$||Li cells, symmetrical cells, Li-ion cells at 20 °C and 40 °C over the course of 25 cycles; and SEM images of graphite surfaces after various cycles (PDF)

■ AUTHOR INFORMATION

Corresponding Authors

Yong Yang − *State Key Laboratory of Physical Chemistry of Solid Surfaces, Department of Chemistry, College of Chemistry and Chemical Engineering, Xiamen University, Xiamen 361005, P.R. China;* orcid.org/0000-0003-1145-8992; Email: yyang@xmu.edu.cn

Jie Li − *Department of Energy, Politecnico di Milano, Milano 20156, Italy;* orcid.org/0000-0002-5131-4769; Email: jie1.li@polimi.it

Authors

Jan-Paul Brinkmann − *Helmholtz-Institute Münster, IEK-12, Forschungszentrum Jülich GmbH, Münster 48149, Germany*

Niloofar Ehteshami-Flammer − *MEET Battery Research Center, Institute of Physical Chemistry, University of Münster, Münster 48149, Germany*

Mingzeng Luo − *State Key Laboratory of Physical Chemistry of Solid Surfaces, Department of Chemistry, College of Chemistry and Chemical Engineering, Xiamen University, Xiamen 361005, P.R. China*

Marco Leißing − *MEET Battery Research Center, Institute of Physical Chemistry, University of Münster, Münster 48149, Germany*

Stephan Röser − *MEET Battery Research Center, Institute of Physical Chemistry, University of Münster, Münster 48149, Germany; E-Lyte Innovations GmbH, Münster 48149, Germany*

Sascha Nowak − *MEET Battery Research Center, Institute of Physical Chemistry, University of Münster, Münster 48149, Germany;* orcid.org/0000-0003-1508-6073

Martin Winter − *Helmholtz-Institute Münster, IEK-12, Forschungszentrum Jülich GmbH, Münster 48149, Germany; MEET Battery Research Center, Institute of Physical Chemistry, University of Münster, Münster 48149, Germany*

Complete contact information is available at: https://pubs.acs.org/10.1021/acsaem.1c01879

Notes

The authors declare no competing financial interest.

■ ACKNOWLEDGMENTS

The authors kindly acknowledge German Research Foundation (DFG, project Li 2916/2-1) and National Natural Science Foundation of China (NSFC, project No. 21761132030) for the funding support through joint Sino-German research project.

■ REFERENCES

(1) Placke, T.; Kloepsch, R.; Dühnen, S.; Winter, M. Lithium ion, lithium metal, and alternative rechargeable battery technologies: the odyssey for high energy density. *J. Solid State Electrochem.* **2017**, *21*, 1939−1964.

(2) Arinicheva, Y.; Wolff, M.; Lobe, S.; Dellen, C.; Fattakhova-Rohlfing, D.; Guillon, O.; Böhm, D.; Zoller, F.; Schmuch, R.; Li, J., Advanced ceramics for energy conversion and storage. In *Advanced Ceramic Materials*, Elsevier: 2020; pp. 549−709.

(3) Schmuch, R.; Wagner, R.; Hörpel, G.; Placke, T.; Winter, M. Performance and cost of materials for lithium-based rechargeable automotive batteries. *Nat. Energy* **2018**, *3*, 267−278.

(4) Lee, W.; Muhammad, S.; Sergey, C.; Lee, H.; Yoon, J.; Kang, Y.-M.; Yoon, W.-S. Advances in the Cathode Materials for Lithium Rechargeable Batteries. *Angew. Chem., Int. Ed.* **2020**, *59*, 2578−2605.

(5) Reed, J.; Ceder, G. Role of Electronic Structure in the Susceptibility of Metastable Transition-Metal Oxide Structures to Transformation. *Chem. Rev.* **2004**, *104*, 4513−4533.

(6) Eilers-Rethwisch, M.; Winter, M.; Schappacher, F. M. Synthesis, electrochemical investigation and structural analysis of doped $Li[Ni_{0.6}Mn_{0.2}Co_{0.2-x}M_x]O_2$ (x = 0, 0.05; M = Al, Fe, Sn) cathode materials. *J. Power Sources* **2018**, *387*, 101−107.

(7) Yue, L.; Ma, C.; Yan, S.; Wu, Z.; Zhao, W.; Liu, Q.; Luo, Y.; Zhong, B.; Zhang, F.; Liu, Y. Improving the intrinsic electronic conductivity of $NiMoO_4$ anodes by phosphorous doping for high lithium storage. *Nano Res.* **2021**, 1−9.

(8) Wentker, M.; Greenwood, M.; Asaba, M. C.; Leker, J. A raw material criticality and environmental impact assessment of state-of-the-art and post-lithium-ion cathode technologies. *J. Energy Storage* **2019**, *26*, No. 101022.

(9) Dühnen, S.; Betz, J.; Kolek, M.; Schmuch, R.; Winter, M.; Placke, T. Toward Green Battery Cells: Perspective on Materials and Technologies. *Small Methods* **2020**, *4*, No. 2000039.

(10) Lee, J.; Seo, D.-H.; Balasubramanian, M.; Twu, N.; Li, X.; Ceder, G. A new class of high capacity cation-disordered oxides for rechargeable lithium batteries: Li−Ni−Ti−Mo oxides. *Energy Environ. Sci.* **2015**, *8*, 3255−3265.

(11) Wang, R.; Li, X.; Liu, L.; Lee, J.; Seo, D.-H.; Bo, S.-H.; Urban, A.; Ceder, G. A disordered rock-salt Li-excess cathode material with high capacity and substantial oxygen redox activity: $Li_{1.25}Nb_{0.25}Mn_{0.5}O_2$. *Electrochem. Commun.* **2015**, *60*, 70−73.

(12) Zhou, K.; Zheng, S.; Liu, H.; Zhang, C.; Gao, H.; Luo, M.; Xu, N.; Xiang, Y.; Liu, X.; Zhong, G.; Yang, Y. Elucidating and Mitigating the Degradation of Cationic-Anionic Redox Processes in $Li_{1.2}Mn_{0.4}Ti_{0.4}O_2$ Cation-Disordered Cathode Materials. *ACS Appl. Mater. Interfaces* **2019**, *11*, 45674−45682.

(13) Lee, J.; Urban, A.; Li, X.; Su, D.; Hautier, G.; Ceder, G. Unlocking the potential of cation-disordered oxides for rechargeable lithium batteries. *Science* **2014**, *343*, 519−522.

(14) Urban, A.; Lee, J.; Ceder, G. The Configurational Space of Rocksalt-Type Oxides for High-Capacity Lithium Battery Electrodes. *Adv. Energy Mater.* **2014**, *4*, No. 1400478.

(15) Glazier, S. L.; Li, J.; Zhou, J.; Bond, T.; Dahn, J. R. Characterization of Disordered $Li_{(1+x)}Ti_{2x}Fe_{(1-3x)}O_2$ as Positive Electrode Materials in Li-Ion Batteries Using Percolation Theory. *Chem. Mater.* **2015**, *27*, 7751−7756.

(16) Assat, G.; Tarascon, J.-M. Fundamental understanding and practical challenges of anionic redox activity in Li-ion batteries. *Nat. Energy* **2018**, *3*, 373−386.
(17) Clément, R.; Lun, Z.; Ceder, G. Cation-disordered rocksalt transition metal oxides and oxyfluorides for high energy lithium-ion cathodes. *Energy Environ. Sci.* **2020**, *13*, 345−373.
(18) Yabuuchi, N. Material Design Concept of Lithium-Excess Electrode Materials with Rocksalt-Related Structures for Rechargeable Non-Aqueous Batteries. *Chem. Rec.* **2019**, *19*, 690−707.
(19) Yabuuchi, N.; Nakayama, M.; Takeuchi, M.; Komaba, S.; Hashimoto, Y.; Mukai, T.; Shiiba, H.; Sato, K.; Kobayashi, Y.; Nakao, A.; Yonemura, M.; Yamanaka, K.; Mitsuhara, K.; Ohta, T. Origin of stabilization and destabilization in solid-state redox reaction of oxide ions for lithium-ion batteries. *Nat. Commun.* **2016**, *7*, 1−10.
(20) Yabuuchi, N.; Takeuchi, M.; Nakayama, M.; Shiiba, H.; Ogawa, M.; Nakayama, K.; Ohta, T.; Endo, D.; Ozaki, T.; Inamasu, T.; Sato, K.; Komaba, S. High-capacity electrode materials for rechargeable lithium batteries: Li_3NbO_4-based system with cation-disordered rocksalt structure. *Proc. Natl. Acad. Sci. U. S. A.* **2015**, *112*, 7650−7655.
(21) Luo, M.; Zheng, S.; Wu, J.; Zhou, K.; Zuo, W.; Feng, M.; He, H.; Liu, R.; Zhu, J.; Zhao, G. Identifying the anionic redox activity in cation-disordered $Li_{1.25}Nb_{0.25}Fe_{0.50}O_2$/C oxide cathodes for Li-ion batteries. *J. Mater. Chem. A* **2020**, *8*, 5115−5127.
(22) Takeda, N.; Ikeuchi, I.; Natsui, R.; Nakura, K.; Yabuuchi, N. Improved Electrode Performance of Lithium-Excess Molybdenum Oxyfluoride: Titanium Substitution with Concentrated Electrolyte. *ACS Appl. Energy Mater.* **2019**, *2*, 1629−1633.
(23) Yim, T.; Kwon, M.-S.; Mun, J.; Lee, K. T. Room Temperature Ionic Liquid-based Electrolytes as an Alternative to Carbonate-based Electrolytes. *Isr. J. Chem.* **2015**, *55*, 586−598.
(24) Theivaprakasam, S.; MacFarlane, D. R.; Mitra, S. Electrochemical studies of N-Methyl N-Propyl Pyrrolidinium bis-(trifluoromethanesulfonyl) imide ionic liquid mixtures with conventional electrolytes in $LiFePO_4$/Li cells. *Electrochim. Acta* **2015**, *180*, 737−745.
(25) Cekic-Laskovic, I.; von Aspern, N.; Imholt, L.; Kaymaksiz, S.; Oldiges, K.; Rad, B. R.; Winter, M. Synergistic effect of blended components in nonaqueous electrolytes for lithium ion batteries. *Top. Curr. Chem.* **2017**, *375*, 1−64.
(26) Gallus, D. R.; Wagner, R.; Wiemers-Meyer, S.; Winter, M.; Cekic-Laskovic, I. New insights into the structure-property relationship of high-voltage electrolyte components for lithium-ion batteries using the pKa value. *Electrochim. Acta* **2015**, *184*, 410−416.
(27) Nölle, R.; Beltrop, K.; Holtstiege, F.; Kasnatscheew, J.; Placke, T.; Winter, M. A reality check and tutorial on electrochemical characterization of battery cell materials: How to choose the appropriate cell setup. *Mater. Today* **2020**, *32*, 131−146.
(28) Aiken, C.; Xia, J.; Wang, D. Y.; Stevens, D.; Trussler, S.; Dahn, J. An apparatus for the study of in situ gas evolution in Li-Ion pouch cells. *J. Electrochem. Soc.* **2014**, *161*, No. A1548.
(29) Gauthier, R.; Hall, D. S.; Taskovic, T.; Dahn, J. R. A Joint DFT and Experimental Study of an Imidazolidinone Additive in Lithium-Ion Cells. *J. Electrochem. Soc.* **2019**, *166*, A3707−A3715.
(30) Leißing, M.; Winter, M.; Wiemers-Meyer, S.; Nowak, S. A method for quantitative analysis of gases evolving during formation applied on $LiNi_{0.6}Mn_{0.2}Co_{0.2}O_2$||natural graphite lithium ion battery cells using gas chromatography-barrier discharge ionization detector. *J. Chromatogr. A* **2020**, *1622*, No. 461122.
(31) Bieker, G.; Winter, M.; Bieker, P. Electrochemical in situ investigations of SEI and dendrite formation on the lithium metal anode. *Phys. Chem. Chem. Phys.* **2015**, *17*, 8670−8679.
(32) McCalla, E.; Sougrati, M. T.; Rousse, G.; Berg, E. J.; Abakumov, A.; Recham, N.; Ramesha, K.; Sathiya, M.; Dominko, R.; Van Tendeloo, G.; Novák, P.; Tarascon, J.-M. Understanding the Roles of Anionic Redox and Oxygen Release during Electrochemical Cycling of Lithium-Rich Layered Li_4FeSbO_6. *J. Am. Chem. Soc.* **2015**, *137*, 4804−4814.
(33) Gao, X.-W.; Feng, C.-Q.; Chou, S.-L.; Wang, J.-Z.; Sun, J.-Z.; Forsyth, M.; MacFarlane, D. R.; Liu, H.-K. $LiNi_{0.5}Mn_{1.5}O_4$ spinel cathode using room temperature ionic liquid as electrolyte. *Electrochim. Acta* **2013**, *101*, 151−157.
(34) Holtstiege, F.; Wilken, A.; Winter, M.; Placke, T. Running out of lithium? A route to differentiate between capacity losses and active lithium losses in lithium-ion batteries. *Phys. Chem. Chem. Phys.* **2017**, *19*, 25905−25918.
(35) Freunberger, S. A.; Chen, Y.; Peng, Z.; Griffin, J. M.; Hardwick, L. J.; Bardé, F.; Novák, P.; Bruce, P. G. Reactions in the Rechargeable Lithium−O_2 Battery with Alkyl Carbonate Electrolytes. *J. Am. Chem. Soc.* **2011**, *133*, 8040−8047.
(36) Ji, H.; Urban, A.; Kitchaev, D. A.; Kwon, D.-H.; Artrith, N.; Ophus, C.; Huang, W.; Cai, Z.; Shi, T.; Kim, J. C.; Kim, H.; Ceder, G. Hidden structural and chemical order controls lithium transport in cation-disordered oxides for rechargeable batteries. *Nat. Commun.* **2019**, *10*, 592.
(37) von Aspern, N.; Röschenthaler, G.-V.; Winter, M.; Cekic-Laskovic, I. Fluorine and Lithium: Ideal Partners for High-Performance Rechargeable Battery Electrolytes. *Angew. Chem., Int. Ed.* **2019**, *58*, 15978−16000.
(38) Li, Q.; Wang, Y.; Wang, X.; Sun, X.; Zhang, J.-N.; Yu, X.; Li, H. Investigations on the Fundamental Process of Cathode Electrolyte Interphase Formation and Evolution of High-Voltage Cathodes. *ACS Appl. Mater. Interfaces* **2019**, *12*, 2319−2326.
(39) Zhang, J.-N.; Li, Q.; Wang, Y.; Zheng, J.; Yu, X.; Li, H. Dynamic evolution of cathode electrolyte interphase (CEI) on high voltage $LiCoO_2$ cathode and its interaction with Li anode. *Energy Storage Materials* **2018**, *14*, 1−7.
(40) Chung, H.; Lebens-Higgins, Z.; Sayahpour, B.; Mejia, C.; Grenier, A.; Kamm, G. E.; Li, Y.; Huang, R.; Piper, L. F. J.; Chapman, K. W.; Doux, J.-M.; Meng, Y. S. Experimental considerations to study Li-excess disordered rock salt cathode materials. *J. Mater. Chem. A* **2021**, *9*, 1720−1732.
(41) Renfrew, S. E.; McCloskey, B. D. Residual Lithium Carbonate Predominantly Accounts for First Cycle CO_2 and CO Outgassing of Li-Stoichiometric and Li-Rich Layered Transition-Metal Oxides. *J. Am. Chem. Soc.* **2017**, *139*, 17853−17860.
(42) Niehoff, P.; Winter, M. Composition and Growth Behavior of the Surface and Electrolyte Decomposition Layer of/on a Commercial Lithium Ion Battery $Li_xNi_{1/3}Mn_{1/3}Co_{1/3}O_2$ Cathode Determined by Sputter Depth Profile X-ray Photoelectron Spectroscopy. *Langmuir* **2013**, *29*, 15813−15821.
(43) Hekmatfar, M.; Kazzazi, A.; Eshetu, G. G.; Hasa, I.; Passerini, S. Understanding the Electrode/Electrolyte Interface Layer on the Li-Rich Nickel Manganese Cobalt Layered Oxide Cathode by XPS. *ACS Appl. Mater. Interfaces* **2019**, *11*, 43166−43179.
(44) Niehoff, P.; Passerini, S.; Winter, M. Interface Investigations of a Commercial Lithium Ion Battery Graphite Anode Material by Sputter Depth Profile X-ray Photoelectron Spectroscopy. *Langmuir* **2013**, *29*, 5806−5816.
(45) Placke, T.; Bieker, P.; Lux, S. F.; Fromm, O.; Meyer, H.-W.; Passerini, S.; Winter, M. Dual-ion cells based on anion intercalation into graphite from ionic liquid-based electrolytes. *Z. Phys. Chem.* **2012**, *226*, 391−407.
(46) Klein, S.; Bärmann, P.; Fromm, O.; Borzutzki, K.; Reiter, J.; Fan, Q.; Winter, M.; Placke, T.; Kasnatscheew, J. Prospects and limitations of single-crystal cathode materials to overcome cross-talk phenomena in high-voltage lithium ion cells. *J. Mater. Chem. A* **2021**, *9*, 7546−7555.
(47) Klein, S.; van Wickeren, S.; Röser, S.; Bärmann, P.; Borzutzki, K.; Heidrich, B.; Börner, M.; Winter, M.; Placke, T.; Kasnatscheew, J. Understanding the Outstanding High-Voltage Performance of NCM523||Graphite Lithium Ion Cells after Elimination of Ethylene Carbonate Solvent from Conventional Electrolyte. *Adv. Energy Mater.* **2021**, *11*, No. 2003738.
(48) Winter, M.; Imhof, R.; Joho, F.; Novák, P. FTIR and DEMS investigations on the electroreduction of chloroethylene carbonate-based electrolyte solutions for lithium-ion cells. *J. Power Sources* **1999**, *81-82*, 818−823.
(49) Schmiegel, J.-P.; Leißing, M.; Weddeling, F.; Horsthemke, F.; Reiter, J.; Fan, Q.; Nowak, S.; Winter, M.; Placke, T. Novel In Situ Gas

Formation Analysis Technique Using a Multilayer Pouch Bag Lithium Ion Cell Equipped with Gas Sampling Port. *J. Electrochem. Soc.* **2020**, *167*, No. 060516.
(50) Jung, R.; Metzger, M.; Maglia, F.; Stinner, C.; Gasteiger, H. A. Oxygen Release and Its Effect on the Cycling Stability of $LiNi_xMn_yCo_zO_2$(NMC) Cathode Materials for Li-Ion Batteries. *J. Electrochem. Soc.* **2017**, *164*, A1361−A1377.
(51) Metzger, M.; Strehle, B.; Solchenbach, S.; Gasteiger, H. A. Origin of H_2 evolution in LIBs: H_2O reduction vs. electrolyte oxidation. *J. Electrochem. Soc.* **2016**, *163*, No. A798.

https://doi.org/10.1021/acsaem.1c01879
ACS Appl. Energy Mater. 2021, 4, 10909−10920